PCCP

Accepted Manuscript

ROYAL SOCIETY OF CHEMISTRY

www.rsc.org/pccp

Journal Name

RSCPublishing

COMMUNICATION

Effect of Metal Doping, Doped Structure, and Annealing under Argon on the Properties of 30-nm Thick Ultrathin Hematite Photoanodes

Cite this: DOI: 10.1039/x0xx00000x

Received 00th January 2012,
Accepted 00th January 2012

DOI: 10.1039/x0xx00000x

www.rsc.org/

Tae-Ho Kim, Hyun Sung Kim, In-Chul Hwang, Kyung Byung Yoon*

The doping of the whole hematite layer with W (9.4%) and the additional doping of the bottom half of the W-doped hematite layer with Sn (8.6%), and the subsequent annealing under argon at 600 °C give rise to large increases in the Fe^{2+} concentration (by >~200 times), carrier density (C_d, by ~48 times) and current density (i_d, by ~8 times at 1.23 V vs. RHE, under 1 sun) with respect to those of bare hematite photoanodes. The measured i_d (0.9 mA cm^{-2}) is the highest among the ultrathin hematite photoanodes and the measured C_d (3.8×10^{22} cm^{-3}) is highest among those ever observed from hematite.

Photoelectrochemical water splitting is one of the most promising routes to convert solar energy to chemical energy. Since water oxidation is more difficult than water reduction, more efforts have been directed at the development of photoanodes with high energy conversion efficiencies. Among various materials that have been tested for photoanodes, hematite (α-Fe_2O_3) has received great attention due to its abundance, the appropriate band gap energy (~2.2 eV) with the valence band edge positioned below the water oxidation potential, and its chemical stability in most electrolytes.[1-45] However, its performance has not been satisfactory due to its unfavorable intrinsic properties such as poor carrier density, very short exciton lifetime (~10 ps), very short hole (h^+) diffusion length (2-4 nm), the Mott insulator type poor electron conductivity, very poor water oxidation reaction kinetics at the semiconductor-electrolyte interface, and the necessity of external potential biases arising from the mismatches of band edge positions.[1-45] Thus, hematite has many intrinsic drawbacks to be applied as such for practically useful photoanodes. In that respect, various strategies have been experimented to use hematite as the photoanode material by overcoming the unfavorable intrinsic properties.[1-45]

The strategies include doping of hematite with various other elements to improve its charge carrier density (C_d),[1-23] control of the morphology or nanostructure of the film to increase the

*Korea Center for Artificial Photosynthesis, Center for Nanomaterials, Department of Chemistry, Sogang University, Seoul 121-742, Korea.
E-mail: yoonkb@sogang.ac.kr; Fax: +82-2-706-4269

Broader Context

Photoelectrochemical water oxidation with hematite (α-Fe_2O_3) as photoanodes has received great attention due to the abundance of the material and its appropriate band gap energy, and others. However, its performance has generally been very poor due to its unfavorable intrinsic properties including the poor carrier density. Doping of the whole or a half layer with various elements have been extensively studied as a means to improve the carrier density. To avoid complex problems associated with thick hematite films, such fundamental studies should be conducted with ultrathin (~30 nm) hematite films. However the examples are rare. We now report that the doping of the top half layer with W and the bottom half layer with W and Sn and the subsequent annealing of the film under an inert gas atmosphere give rise to large increases in the Fe^{2+}concentration (by more than ~200 times), carrier density (by ~48 times) and current density (by ~8 times) with respect to those of bare hematite photoanodes. The measured carrier density (3.8×10^{22} cm^{-3}) is highest among those observed from hematite. This finding will serve as a guideline to improve the performance of hematite photoanodes.

surface area,[1,4,5,8-11,14,18-32] introduction of an intermediate layer at the interface between the hematite and the underlying transparent conducting oxide (typically F-doped tin oxide, FTO)[33-36] to enhance the hole transport process[33,34] and to control the crystallinity of the hematite layer,[35] and introduction of a catalytically active[24,37,38] or surface-state passivating layer[2] on top of the hematite layer to increase the charge transfer rate at the solid-liquid interface between the photoanode and water. Among these, the improvement in C_d is most crucial for hematite to be applied for practically viable photoanodes. In this respect, more efforts should be directed at the finding of novel doping elements and novel doped hematite structures that can lead to a significant increase in C_d. Efforts should also be directed at the elucidations of the reasons for the doping-induced increase in C_d, and the relationship between C_d and the photocurrent density (i_d) and between C_d and onset potentials.

Such studies can be carried out with thick (> 50 nm) hematite photoanodes. However, as the thickness increases many complex factors such as the grain size, surface defects on each grain, the intergrain charge hoping kinetics, mismatch of the grain orientations, the degree of homogeneous distribution of doped elements within the hematite film, the degree of homogeneous distribution of valence charges of Fe and doped elements within the hematite film, and others simultaneously affect the overall electronic properties, which eventually obscure the analyses of the intrinsic doping-induced change of the electronic properties. However, due to the practical difficulties associated with dealing with ultrathin hematite films, only a few research groups have actually carried out the fundamental studies of hematite photoanodes using ultrathin hematite films.[16,17,33,-36]

Among the studies with ultrathin hematite films, a majority has addressed the effect of under layer coating on i_d[33,-36] rather than the effect of doping material and the doped structure on C_d and their subsequent effects on i_d. Even in such cases where the effects of doping and doped structure on i_d were addressed, only Ti[16] and Mg[17] have been chosen as the doping elements and the effect of splitting of the hematite layer into the Mg-doped top layer (p-type semiconductor) and bare hematite bottom layer (n-type semiconductor)[17] on i_d was measured. Thus, the systematic searches for other doping elements and the effects of co-doping of two elements into ultrathin hematite films and the splitting of ultrathin hematite films into a more complex double layers consisting of a single metal-doped top layer and a two metal-co-doped bottom layer on C_d have not been carried out.

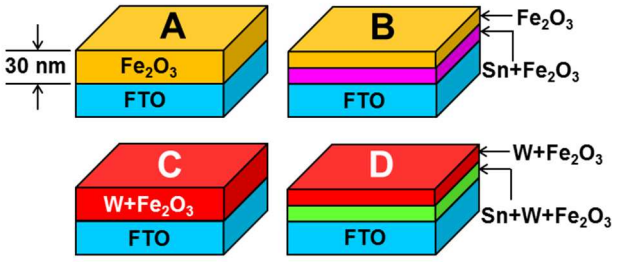

Fig. 1 Schematic illustration of the four hematite photoanodes prepared and studied in this work.

During the study of doping-induced change of electronic properties of ultrathin hematite films, the following points should be addressed. The first is how high i_d can be increased by only doping and by varying the doped structures (without the help of the under layer coating). This result is important to re-evaluate the advantage of doping and the doped structure. The second is to understand the reasons for the doping-induced change in C_d and its effect on i_d. The systematic studies on this issue have not been carried out using ultrathin hematite films and the elucidation of such information will be of great value to understand the fundamental aspects regarding the doping-induced change of electronic properties of hematite. The third is to study the effects of the annealing gas, Ar and air, on C_d and i_d of ultrathin hematite photoanodes. The result obtained from this will be a good complementary to the recent finding with a thick hematite photoanode that the inert gas suppresses the growth of small hematite grains into larger grains, which in turn gives rise to higher i_d.[22] The fourth is to see whether magnetron sputters can also be employed for such systematic studies. Knowing that only spray pyrolysis,[33-35] atomic layer deposition,[16,17] and electron beam sputtering[36] have been employed to prepare ultrathin hematite films, the demonstration of the capability of magnetron sputtering for such purposes is of great practical value because magnetron sputtering is the most convenient method to deposit thin films of various metal oxides and metals on various substrates.

We prepared four types of hematite photoanodes, a pure hematite photoanode ($[Fe_2O_3]$), a hematite photoanode consisting of a pure hematite layer as the top half layer and a Sn-doped (8.64%) hematite layer as the bottom half layer (denoted as $[Fe_2O_3]_t/[Sn+Fe_2O_3]_b$), a W-doped (9.43%) hematite photoanode (denoted as $[W+Fe_2O_3]$), and a hematite photoanode consisting of a W-doped hematite layer as the top half layer and a Sn- and W-co-doped (8.64 and 9.43%) hematite layer as the bottom half layer (denoted as $[W+Fe_2O_3]_t/[Sn+W+Fe_2O_3]_b$) using a magnetron sputtering system consisting of a RF magnetron gun and two DC magnetron guns. These hematite photoanodes are schematically illustrated in Fig. 1. They are also simply denoted as A, B, C, D, respectively. A hematite target was mounted on the RF magnetron gun and W and Sn targets were mounted on DC magnetron guns. The chamber ambient gas was Ar. The thicknesses were fixed to 30 nm. The photoanodes were annealed at various temperatures between 300 and 800 °C under Ar and air, respectively. The annealing periods were 3 h at the temperatures between 300 and 600 °C and 5-10 min at 700 and 800 °C.

Because the hematite films are very thin, the scanning electron microscope images did not show much difference except slight changes in the surface textures. However, their X-ray diffraction patterns (Fig. 2a) confirmed that they are indeed hematite films. The diffraction patterns were obtained by subtracting the diffraction pattern of each photoanode with that of a bare FTO glass. The presence of A_{1g} (225 and 498 cm^{-1}) and E_g (247, 293,

299, 412, 613 cm^{-1}) bands in Raman spectra (Fig. 2b) further confirmed that the films are hematite.[15,32] Although weak, a broad additional band centred at ~660 cm^{-1}, the peak that arises due to defect sites, could also be identified in all cases. Thus, highly crystalline bare and metal-doped single and double layered ultrathin hematite films can be readily deposited on FTO glass by magnetron sputtering. The thicknesses were readily controlled by utilizing the linear relationships obtained between the thickness and the absorbance of the film and the sputtered time and the thickness. The 30-nm thick hematite films were chosen and their results were compared because they gave highest i_d values at 1.23 V (vs RHE).

The I-V curves of the four photoanodes under the 1 sun condition (AM 1.5, 100 mW cm^{-2}) are compared in Fig. 3a. These photoanodes were deposited and annealed at 600 °C under Ar. The onset potentials (V_{on}) of the four photoanodes A, B, C, and D were 0.84, 0.66, 0.64, and 0.60 V (vs. RHE), respectively. Thus, a large (240 mV) shift of V_{on} was observed on going from A to D.

The temperature and the nature of the gas during annealing sensitively affect the performance of the photoanode. Thus, when photoanodes were annealed at lower or higher than 600 °C under Ar, the i_d values at 1.23 V (vs RHE) decreased. For example, in the case of D, when the annealing temperatures under Ar were 300, 400, 500, 550, 700, and 800 °C, the i_d values at 1.23 V (vs RHE) were 0.07, 0.18, 0.81, 0.85, 0.87, and 0.84. Also, if annealed at 600 °C under air the i_d value at 1.23 V (vs RHE) was 0.69 mA cm^{-2}. Therefore, the C_d and i_d values of the ultrathin hematite photoanodes that were annealed at 600 °C under Ar are compared in this work.

The measured i_d values of A, B, C, and D at 1.23 V (vs. RHE) were 0.12, 0.41, 0.66, and 0.90 mA cm^{-2}, respectively. They were compared with those of reported ultrathin hematite photoanodes in Fig. 3b. Note that the i_d values of C and D are higher than the reported highest value (0.5 mA cm^{-2}) obtained from ultrathin hematite photoanodes,[16,17,33-36] despite the fact that there were no under layer and top layer coatings and no morphology variation by nanostructuring. The Mott-Schottky plots of A, B, C, and D are shown in Fig. 3c. The calculated C_d values were 7.9×10^{20}, 4.6×10^{21}, 1.2×10^{22}, and 3.8×10^{22} cm^{-3}, respectively, or 1.3, 7.6, 19.9, and 63.1 mmol cm^{-3}, respectively. In fact, the C_d value of D (3.8×10^{22} cm^{-3} or 63.1 mmol cm^{-3}) is larger than the reported highest value (1.3×10^{22} cm^{-3} or 21.5 mmol cm^{-3}) observed from 700-nm thick 10% Al-doped hematite photoanode[6] by ~3 times. Even the C_d value of the W-doped ultrathin hematite photoanode (1.2×10^{22} cm^{-3}, 19.9 mmol cm^{-3}) is comparable with that of the reported highest value.

As noted, C_d increases by 5.8 times (from 7.9×10^{20} to 4.6×10^{21} cm^{-3}) on going from A to B. Simultaneously, i_d increases by 3.4 times (from 0.12 to 0.41 mA) on going from A to B. Upon going from A to C, C_d increases by 15.2 times (from 7.9×10^{20} to 1.2×10^{22} cm^{-3}) and i_d increases by 5.5 times (from 0.12 to 0.66 mA). Upon going from C to D, C_d increases by 3.2 times (from 1.2×10^{22} to 3.8×10^{22} cm^{-3}) and i_d increases by 1.4 times (from 0.66 to 0.9 mA). Upon going from B to D, C_d increases by 8.3 times (from 4.6×10^{21} to 3.8×10^{22} cm^{-3}) and i_d increases by 2.2 times (from 0.66 to 0.9 mA). Lastly, upon going from A to D, C_d increases by 48.1 times (from 7.9×10^{20} to 3.8×10^{22} cm^{-3}) and i_d increases by 7.5 times (from 0.12 to 0.90 mA).

Thus, the splitting of an ultrathin hematite layer into two layers by doping the bottom half with Sn (A→B and C→D) gives rise to

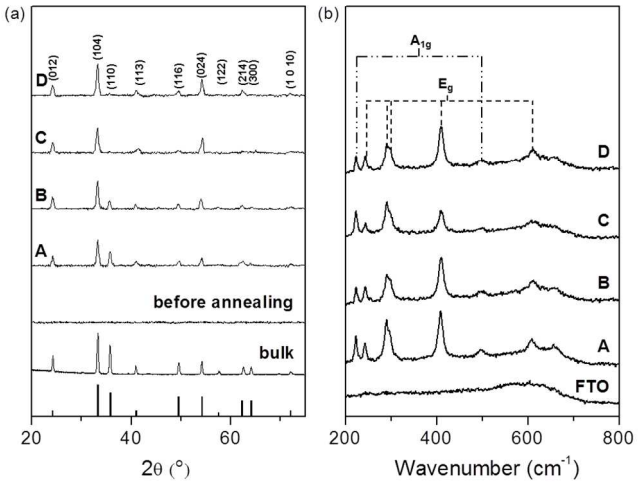

Fig. 2 (a) X-ray diffraction patterns of a bulk hematite powder, 30-nm thick amorphous Fe_2O_3 film (as indicated), $[Fe_2O_3]$ (A), $[Fe_2O_3]_l/[Sn+Fe_2O_3]_b$ (B), $[W+Fe_2O_3]$ (C), and $[W+Fe_2O_3]_l/[Sn+W+Fe_2O_3]_b$ (D). (b) Raman spectra of bare FTO (as indicated), $[Fe_2O_3]$ (A), $[Fe_2O_3]_l/[Sn+Fe_2O_3]_b$ (B), $[W+Fe_2O_3]$ (C), and $[W+Fe_2O_3]_l/[Sn+W+Fe_2O_3]_b$ (D). A, B, C, and D in (a) and (b) were annealed at 600 °C for 3 h under Ar.

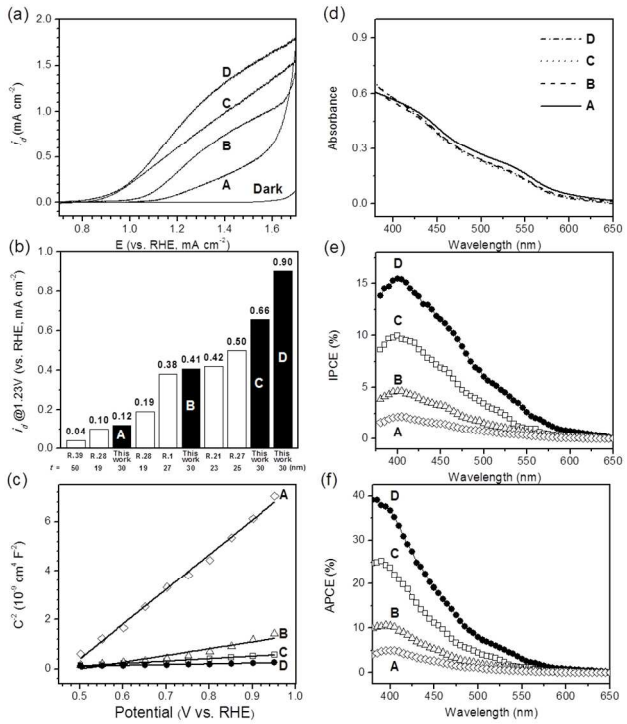

Fig. 3 (a) I-V curves of A, B, C, and D under 1 sun condition. (b) Comparison of current densities (i_d) of A, B, C, and D at 1.23 V (vs. RHE) with those of the reported results. (c) The Mott-Schottky plots of A, B, C, and D. (d) Background-subtracted UV-vis spectra of A, B, C, and D. (e) IPCE spectra of A, B, C, and D.(f) APCE spectra of A, B, C, and D. A, B, C, and D in (a-f) were annealed at 600 °C for 3 h under argon.

the increases in C_d and i_d. This phenomenon can be likened to the doping of the hematite photoanode with Sn through migration of Sn from the FTO glass to the hematite layer during high temperature (700-800 °C) annealing, giving rise to a substantial increase in i_d. Furthermore, doping of the hematite layers with W (A→C and B→D) also gives rise to marked increases in C_d and i_d. Accordingly, the mixing of the two effects, doping and double layer splitting, (A→D) gives rise to dramatic increases in C_d and i_d (by 48.1 and 7.5 times, respectively). It is also important to note that this type of systematic research can be done with 30-nm thick hematite photoanodes. Thus, this result shows that even with 30-nm thick hematite films there are large rooms to study the effect of various metal doping and double layer splitting on C_d and i_d.

In the case of double layer splitting, the choice of the double layer ordering is very important to achieve high efficiencies. For example the i_d values at 1.23 V (vs. RHE) became very low in the cases of $[W+Fe_2O_3]_t/[Sn+Fe_2O_3]_b$, $[Sn+W+Fe_2O_3]_t/[Fe_2O_3]_b$, $[Fe_2O_3]_t/[Sn+W+Fe_2O_3]_b$, $[Sn+W+Fe_2O_3]_t/[W+Fe_2O_3]_b$, $[Sn+Fe_2O_3]_t/[W+Fe_2O_3]_b$, $[Sn+W+Fe_2O_3]_t/[Sn+Fe_2O_3]_b$, $[Sn+Fe_2O_3]_t/[W+Sn+Fe_2O_3]_b$, and $[Fe_2O_3]_t/[W+Fe_2O_3]_b$, which are 0.01, 0.02, 0.07, 0.08, 0.11, 0.11, 0.19, 0.44, respectively.

There were several reports in which thick hematite photoanodes were prepared with magnetron sputtering.[39-41] The observed i_d values from these photoanodes were very low (0.01-0.1 mA cm^{-2}), giving the impression that the magnetron sputtering is not desirable for this type of study. In this respect, this work also demonstrates that the magnetron sputtering is in fact a highly capable and versatile tool to prepare high quality ultrathin hematite photoanodes doped with a single or multiple metals.

The UV-vis spectra of the four photoanodes are nearly the same (Fig. 3d). However, the intensities of their IPCE (incident photon to current conversion efficiency) spectra (at 1.23 V vs RHE) were markedly different (Fig. 3e). All IPCE spectra became identical when the intensities were normalized and the maximum values were obtained at 400 nm. In the case of D, the highest IPCE value was 16% at 400 nm (at 1.23 V vs RHE). The corresponding APCE spectra are shown in Fig. 3f. In the case of D, the APCE value is also the record high (38% at 400 nm, at 1.23 V vs RHE, under 1 sun) among the reported values from ultrathin hematite photonodes (~20% at 1.43 V,[34] ~20% at 1.0 V,[17] ~32% at 1.43 V[33] vs. RHE).

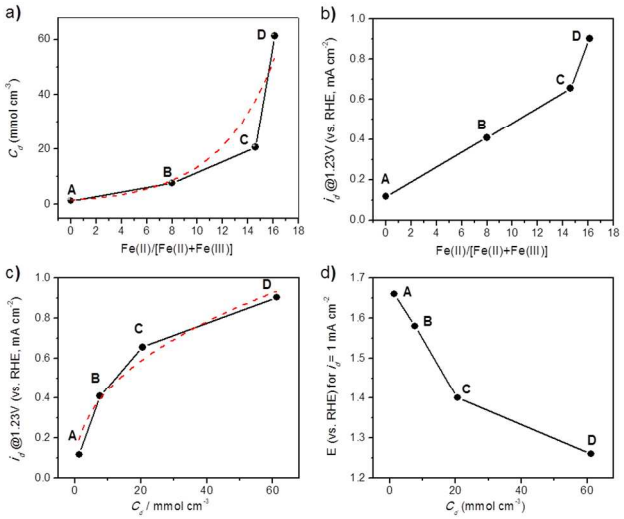

Fig. 4 (a) The relationships between Fe(II)/[Fe(II)+Fe(III)] and C_d (a), between Fe(II)/[Fe(II)+Fe(III)] and i_d (b), between C_d and i_d at 1.23 V (vs. RHE) (c), and between C_d and the potential E (vs. RHE) at which i_d = 1 mA (d).

From the X-ray photoelectron spectroscopy (XPS) data of the four photoanodes we extracted the Fe(II) percentage {Fe(II)/[(Fe(II)+Fe(III)]} × 100, or %Fe(II). The observed %Fe(II) for A, B, C, and D were 0, 0.087, 0.171, and 0.192 respectively. Thus, upon doping the whole hematite layer with W (A to C and B to D) or doping the bottom half layer with Sn, %Fe(II) increased.

As %Fe(II) increases C_d also increased in a manner shown in Fig. 4a. The relationship between %Fe(II) and C_d can be formulated as $C_d = 1.46 \times (1.25)^{\%Fe(II)}$. As %Fe(II) increases i_d (at 1.23 V vs. RHE) also increases (Fig. 4b). The relationship between C_d and i_d is shown in Fig. 4(c). This relationship can be formulated as $i_d = 0.169 \times C_d^{0.416}$. The relationship between the potential at which i_d = 1 mA (V@1 mA) is shown in Fig. 4d. Thus, as C_d increases, the V@1 mA decreases significantly.

The above data clearly show that %Fe(II), C_d, i_d, and V@1 mA are very closely interrelated. This report thus unambiguously demonstrates that %Fe(II) is the primary chemical factor that determines the performances of the hematite photoanodes. To increase %Fe(II), the W- and/or Sn-doped hematites should be annealed under the inert gas atmosphere. Otherwise, %Fe(II) becomes negligible and at the same time C_d and i_d become very small. In this sense, the role of W and Sn is to convert a fraction of $Fe(III)_2O_3$ to Fe(II)O as shown in eq. 1

$$Fe(III)_2O_3 + M_x \rightarrow [2Fe(II)O]_x[Fe(III)_2O_3]_{1-x} + MO_x \qquad (1)$$

Therefore, to make the above reaction undergo during annealing it should be carried out under an inert gas atmosphere. The doping of hematite with metals during the film deposition should also be carried out in the inert gas atmosphere. Since WO_3 is a much better photoanode than Fe_2O_3 and WO_3 and SnO_2/SnO are much better conductors than Fe_2O_3, the resulting WO_3, SnO_2, and SnO from eq 1 may also contribute to the enhancement of the performances of photoanodes B, C, and D. However, the absence of diffractions of WO_3, SnO_2, and SnO in the X-ray diffraction and the Raman shifts in Fig. 2 indicates that the grain sizes of the produced MO_x are either too small to be detected or they exist as noncrystalline amorphous materials. In either case, the contribution of the superior conductivity of WO_3, SnO_2, and SnO and the superior photoanode property of WO_3 to the enhancement of the photoanode performance in B, C, and D is expected to be minimal.

Conclusions

The doping of 30-nm thick ultrathin hematite with W and/or Sn leads to the increase in %Fe(II), which in turn gives rise to increases in C_d and i_d. Thus, %Fe(II), C_d, and i_d are closely related. The relationship between C_d and %Fe(II) can be expressed as $C_d = 1.46 \times (1.25)^{\%Fe(II)}$. The relationship between i_d and C_d can be expressed as $i_d = 0.169 \times C_d^{0.416}$. As %Fe(II) increases C_d increases and as C_d increases i_d increases in such manners described above. The doping of the whole 30-nm thick hematite layer with W and the doping of the bottom half layer of the ultrathin hematite layer with Sn give rise to large increases in %Fe(II) and hence, C_d and i_d. The combining of doping the whole film with W and selective doping of the bottom half with Sn gives rise to a marked increase in C_d (by 48.1 times) and i_d (by 7.5 times) with respect to those of bare hematite photonanodes. Even with 30-nm thick ultrathin hematite photoanodes, i_d (at 1.23 V vs. RHE) can be increased to 0.9 mA cm^{-2} under the 1 sun condition, which is significantly higher than the reported highest value with ultrathin hematite photoanodes. To allow the doped metal to reduce Fe(III) to Fe(II), annealing should be carried out under an inert gas atmosphere. Magnetron sputtering is a very useful and versatile method for the preparation of ultrathin metal doped hematite photoanodes for the fundamental research. Overall, there are much works to be done with the ultrathin hematite films. The fundamental knowledge on the intrinsic electronic properties of hematite acquired in this work will serve as useful guidelines for the fabrication of commercially viable hematite photoanodes in the future.

Acknowledgements

This work was supported by the Korea Center for Artificial Photosynthesis, located at Sogang University and funded by the Ministry of Science, ICT and Future Planning through the National Research Foundation of Korea, No. 2009-0093886 and No. 2012R1A2A3A01009806. We also thank J. Y. Lee for the help in drawing Figures.

Notes and references

1 Kay, I. Cesar, M. Grätzel, J. Am. Chem. Soc., 2006, 128, 15714-15721.
2 F. Le Formal, N. Tétreault, M. Cornuz, T. Moehl, M. Grätzel, K. Sivula, Chem. Sci., 2011, 2, 737.
3 P. Zhang, A. Kleiman-Shwarsctein, Y.-S. Hu, J. Lefton, S. Sharma, A. J. Forman, E. W. McFarland, Energy Environ. Sci., 2011, 4, 1020.
4 Kleiman-Shwarsctein, Y. S. Hu, A. J. Forman, G. D. Stucky, E. W. McFarland, J. Phys. Chem. C, 2008, 112, 15900-15907.
5 D.-D. Qin, C.-L. Tao, S.-i. In, Z.-Y. Yang, T. E. Mallouk, N. Bao, C. A. Grimes, Energy Fuels, 2011, 25, 5257-5263.
6 Kleiman-Shwarsctein, M. N. Huda, A. Walsh, Y. Yan, G. D. Stucky, Y.-S. Hu, M. M. Al-Jassim, E. W. McFarland, Chem. Mater., 2010, 22, 510-517.
7 C. J. Sartoretti, B. D. Alexander, R. Solarska, W. A. Rutkowska, J. Augustynski, R. Cerny, J. Phys. Chem., B 2005, 109, 13685-13692.
8 G. Wang, Y. Ling, D. A. Wheeler, K. E. George, K. Horsley, C. Heske, J. Z. Zhang, Y. Li, Nano Lett., 2011, 11, 3503-3509.
9 S. Saremi-Yarahmadi, K. G. U. Wijayantha, A. A. Tahir, B. Vaidhyanathan, J. Phys. Chem. C, 2009, 113, 4768-4778.
10 Y. S. Hu, A. Kleiman-Shwarsctein, A. J. Forman, D. Hazen, J. N. Park, E. W. McFarland, Chem. Mater., 2008, 20, 3803-3805.
11 Y. Hou, F. Zuo, A. Dagg, P. Feng, Angew. Chem. Int. Ed., 2013, 52, 1248-1252.
12 C. Du, X. Yang, M. T. Mayer, H. Hoyt, J. Xie, G. McMahon, G. Bischoping, D. Wang, Angew. Chem. Int. Ed., 2013, 52, 12692-12695.
13 M. Zhang, W. Luo, Z. Li, T. Yu, Z. Zou, Appl. Phys. Lett., 2010, 97, 042105.
14 F. L. Souza, K. P. Lopes, P. A. P. Nascente, E. R. Leite, Sol. Energy Mater. Sol. Cells, 2009, 93, 362-368.
15 P. Kumar, P. Sharma, R. Shrivastav, S. Dass, V. R. Satsangi, Int. J. Hydrogen Energy, 2011, 36, 2777-2784.
16 Zandi, B. M. Klahr, T. W. Hamann, Energy Environ. Sci., 2013, 6, 634.
17 Y. Lin, Y. Xu, M. T. Mayer, Z. I. Simpson, G. McMahon, S. Zhou, D. Wang, J. Am. Chem. Soc., 2012, 134, 5508-5511.
18 Y. Ling, G. Wang, D. A. Wheeler, J. Z. Zhang, Y. Li, Nano Lett., 2011, 11, 2119-2125.
19 R. Morrish, M. Rahman, J. M. MacElroy, C. A. Wolden, ChemSusChem, 2011, 4, 474-479.
20 K. Sivula, R. Zboril, F. Le Formal, R. Robert, A. Weidenkaff, J. Tucek, J. Frydrych, M. Grätzel, J. Am. Chem. Soc., 2010, 132, 7436-7444.
21 L. Li, Y. Yu, F. Meng, Y. Tan, R. J. Hamers, S. Jin, Nano Lett., 2012, 12, 724-731.
22 L. Wang, C.-Y. Lee, P. Schmuki, J. Mater. Chem. A, 2013, 1, 212.
23 R. Franking, L. Li, M. A. Lukowski, F. Meng, Y. Tan, R. J. Hamers, S. Jin, Energy Environ. Sci., 2013, 6, 500; P. Wang, D. Wang, J. Lin, X. Li, C. Peng, X. Gao, Q. Huang, J. Wang, H. Xu, C. Fan, ACS Appl. Mater. Interfaces, 2012, 4, 2295-2302.
24 J. Y. Kim, G. Magesh, D. H. Youn, J. W. Jang, J. Kubota, K. Domen, J. S. Lee, Sci. Rep., 2013, 3, 2681.
25 R. H. Goncalves, B. H. Lima, E. R. Leite, J. Am. Chem. Soc., 2011, 133, 6012-6019.
26 H. Jun, B. Im, J. Y. Kim, Y.-O. Im, J.-W. Jang, E. S. Kim, J. Y. Kim, H. J. Kang, S. J. Hong, J. S. Lee, Energy Environ. Sci., 2012, 5, 6375.
27 N. T. Hahn, H. C. Ye, D. W. Flaherty, A. J. Bard, C. B. Mullins, ACS Nano, 2010, 4, 1977-1986.
28 S. K. Mohapatra, S. E. John, S. Banerjee, M. Misra, Chem. Mater., 2009, 21, 3048-3055.
29 R. R. Rangaraju, A. Panday, K. S. Raja, M. Misra, J. Phys. D: Appl. Phys., 2009, 42, 135303.
30 Y. Ling, G. Wang, J. Reddy, C. Wang, J. Z. Zhang, Y. Li, Angew. Chem. Int. Ed., 2012, 51, 4074-4079.
31 E. Thimsen, F. Le Formal, M. Grätzel, S. C. Warren, Nano Lett., 2011, 11, 35-43; S. Kumari, A. P. Singh, C. Tripathi, D. Chauhan, S. Dass, R. Shrivastav, V. Gupta, K. Sreenivas, V. R. Satsangi, Int. J. Photoenergy, 2007, 2007, 1-6.

A. Tahir, K. G. U. Wijayantha, S. Saremi-Yarahmadi, M. Mazhar, V. McKee, Chem. Mater., 2009, 21, 3763-3772.
32 T. Hisatomi, H. Dotan, M. Stefik, K. Sivula, A. Rothschild, M. Grätzel, N. Mathews, Adv. Mater., 2012, 24, 2699-2702.
33 F. Le Formal, M. Grätzel, K. Sivula, Adv. Funct. Mater., 2010, 20, 1099-1107.
34 T. Hisatomi, J. Brillet, M. Cornuz, F. Le Formal, N. Tétreault, K. Sivula, M. Grätzel, Faraday Discuss., 2012, 155, 223.
35 H. W. Gao, C. Liu, H. E. Jeong, P. D. Yang, ACS Nano, 2012, 6, 234-240.
36 M. Barroso, A. J. Cowan, S. R. Pendlebury, M. Grätzel, D. R. Klug, J. R. Durrant, J. Am. Chem. Soc., 2011, 133, 14868-14871.
37 D. K. Zhong, M. Cornuz, K. Sivula, M. Grätzel, D. R. Gamelin, Energy Environ. Sci., 2011, 4, 1759.
38 H. Tang, M. A. Matin, H. Wang, T. Deutsch, M. Al-Jassim, J. Turner, Y. Yan, J. Appl. Phys., 2011, 110, 123511.
39 J. A. Glasscock, P. R. F. Barnes, I. C. Plumb, N. Savvides, J. Phys. Chem. C, 2007, 111, 16477-16488.
40 H. Tang, W.-J. Yin, M. A. Matin, H. Wang, T. Deutsch, M. M. Al-Jassim, J. A. Turner, Y. Yan, J. Appl. Phys., 2012, 111, 73502.
41 S. U. M. Khan, J. Akikusa, J. Phys. Chem. B, 1999, 103, 7184-7189.
42 B. Klahr, S. Gimenez, F. Fabregat-Santiago, T. Hamann, J. Bisquert, J. Am. Chem. Soc., 2012, 134, 4294-4302.

Graphic Table of Contents